06

Study of the Effect of a Small Addition of ZrO$_2$ on the Density and Grain Growth of Alumina

© M.S. Boldin,[1] A.A. Popov,[1] A.A. Murashov,[1] N.V. Sakharov,[1] S.V. Shotin,[1] A.V. Nokhrin,[1]
V.N. Chuvil'deev,[1] N.Yu. Tabachkova,[2,3] K.E. Smetanina[1]

[1] Lobachevsky State University of Nizhny Novgorod, Nizhny Novgorod, Russia
[2] National University of Science and Technology MISiS, Moscow, Russia
[3] Prokhorov Institute of General Physics, Russian Academy of Sciences, Moscow, Russia
e-mail: boldin@nifti.unn.ru

The effect of an additive of 0.5 wt.% of zirconium oxide on the spark plasma sintering (SPS) kinetics of alumina powders has been studied. Ceramics were obtained by mixing alumina powders in a planetary mill with grinding media from stabilized zirconium oxide. The activation energy of SPS was estimated using the Young-Cutler model. It has been shown that the density and average grain size in ceramics obtained from submicron alumina powders are significantly affected by the nonequilibrium state of the interfaces formed as a result of the transformation of the amorphous phase present on the alumina powder particle surface. The grain size and density of ceramics obtained from fine powders are significantly affected by the coalescence of ZrO$_2$ particles.

Keywords: Alumina, zirconium oxide, spark plasma sintering, density, diffusion, activation energy.

Introduction

Fine-grained aluminum oxide-based ceramics with an increased content of zirconium oxide particles (20−50% ZrO$_2$) are actively used in general and special machinery [1,2]. Additions of ZrO$_2$ particles provide increased hardness and cracking resistance of aluminum oxide [3,4], so ceramics Al$_2$O$_3$−ZrO$_2$ are widely used to manufacture metal cutting tools, wear resistant friction pairs, stop valves, in special applications, etc. [1,2,5]. The addition of a large volume fraction of ZrO$_2$O$_2$ particles in Al$_2$O$_3$ allows blocking the crack movement by forming compressive internal stresses [3,4,6].

Further prospects for improving the mechanical properties are associated with the possibility of forming a homogeneous ultrafine grained (UFG) microstructure in ceramics [7,8]. This can be achieved through the simultaneous use of nano and submicron powders as starting materials as well as their high-speed sintering techniques. One promising method for obtaining UFG ceramics is the electric pulse („spark") plasma sintering (EPPS) technology, which is a new effective method of high-speed hot pressing [9,10]. The essence of the EPPS technology is the high-speed heating of powders in a graphite mold by passing millisecond pulses of high-power current. The sintering takes place in a vacuum or in an inert environment, under conditions of uniaxial pressure application. High heating rates (up to 2500 °C/min) allow to limit significantly the grain growth rate, and the possibility to change all key parameters of technological process (time and temperature of heating, value of applied pressure, heating and cooling rate) —

effectively control the parameters of microstructure of ceramics [9,10] directly in the EPPS process.

It should be noted that a high density of ceramics can be achieved by higher heating temperatures or prolonged isothermal holding at the sintering temperature, which inevitably leads to grain growth [11,12]. To solve this problem, an approach based on the stabilization of the aluminum oxide microstructure by adding nanoparticles ZrO$_2$ [13,14] is effective.

The aim of this work is to study the mechanism of high-speed sintering of aluminum oxide with a small (0.5 wt.%) content of ZrO$_2$ nanoparticles and the effect of ZrO$_2$ particles on the kinetics of grain growth during EPPS of aluminum oxide. The small content of ZrO$_2$ particles allows minimizing the influence of the factor associated with the influence of internal stresses arising during the reversible transformation (phase transition) of ZrO$_2$ from the monoclinic to the tetragonal phase. The peculiarity of the present work is the production of Al$_2$O$_3$−ZrO$_2$ compositions by milling, which is realized by mixing Al$_2$O$_3$ powders in a planetary mill with zirconium oxide grinding bodies.

1. Materials and methods

The research objects were industrial aluminum oxide powders α-Al$_2$O$_3$ with different dispersion levels — submicron powders (series № 1) produced by Taimei Chemicals Co, Ltd with an initial particle size of $R \sim 0.2$m (brand name TM-DAR) and micron powders (series № 2)

produced by Alfa Aesar - A Johnson Matthey Company ($R \sim 1m$).

Al$_2$O$_3$−ZrO$_2$ powder compositions were obtained by mixing the initial Al$_2$O$_3$ powders in a planetary mill „FRITSCH — Pulverisette 6". Stabilized zirconium oxide (ZrO$_2$−Y$_2$O$_3$) beads were used as grinding bodies with size 0.4−0.6 mm. A Teflon tumbler was used to eliminate the mounding associated with hardware abrasion. Isopropyl alcohol was used as the liquid medium. The ratio of masses of powder, grinding bodies and alcohol was 1 : 4 : 6. The frequency of rotation of the grinding jar was 400 rpm, the duration of mixing was 6 h. Alcohol removal from the powders was performed at 70°C (12 h). The mixing modes selected on the basis of previously conducted studies, provided grinding of zirconium oxide from the grinding bodies and used tooling in the amount of 0.5 wt.% with accuracy ±0.1%.

The EPPS of 12 mm diameter and 3 mm height samples was performed using a Dr. Sinter model SPS-625 (SPS SYNTEX INC. Ltd, Japan). Uniaxial pressure $P = 70$ MPa was applied simultaneously with the beginning of heating. Sintering was carried out in vacuum (6 Pa). Temperature was measured using a CHINO IR-AH2 pyrometer focused on the surface of the graphite mold. Based on the comparison of the readings of the pyrometer (T_{eff}) and the control thermocouple attached to the surface of the sample, the values T_{eff} were recalculated to the sample temperature (T) using empirical relations of the form: $T = aT_{\text{eff}} - b$, where a and b — numerical factors. Remains of graphite from the surface of the samples were removed by annealing in an air furnace (750°C, 1 h) and mechanical polishing. Later , for the sake of brevity, the samples obtained by sintering pure Al$_2$O$_3$ powder of № 1 series and Al$_2$O$_3$−ZrO$_2$ composite prepared on the basis of powder of № 1 series will be called ceramics of № 1 series, series, and the samples obtained by sintering pure Al$_2$O$_3$ powder of № 2 series and the composition of Al$_2$O$_3$−ZrO$_2$ prepared on the basis of № 2 series powder will be called ceramics of № 2 series.

Two sintering modes were used in this work:

— Mode A: heating at a constant rate ($V_h = 10, 50, 100, 250, 350$ and 700°C/min) to the end shrinkage temperature (T_s) or to the set temperature (T_1, T_2, T_3);

— Mode B: heating to a given temperature (T_1, T_2, T_3) at a rate of 50°C/min and sintering at this temperature in the mode of isothermal holding duration (t_s) to 30 min.

The dependence of the effective powder shrinkage (L_{eff}) on the heating temperature was recorded in the EPPS process. To account for the contribution of thermal expansion (L_0), experiments were conducted on the heating of empty molds. The value of true shrinkage was calculated as $L = L_{\text{eff}} - L_0$. The $L(T)$ recalculation into the temperature dependence of compaction (ρ/ρ_{th}) was carried out in accordance with [15].

The density of ceramics (ρ) was measured by hydrostatic weighing in distilled water using Sartorius CPA scales at room temperature. The measurement accuracy ρ was

±0.005 g/cm^3. The theoretical density (ρ_{th}) of Al$_2$O$_3$ and ceramic Al$_2$O$_3$ + 0.5% ZrO$_2$ were taken to be 4.05 and 4.051 g/cm^3 respectively.

Microhardness (H_v) was measured on a hardness tester „Struers Duramin-5" (load 2 kg). The value of the minimum crack resistance coefficient K_{IC} was calculated by the Palmquist method based on the length of the maximum radial crack. When calculating the value of K_{IC}, the modulus of elasticity was taken to be $E = 350$ GPa. The measurement accuracy of H_v and K_{IC} was ±1 GPa and ±0.3 MPa · m$^{1/2}$ respectively.

The sample microstructure was studied using a Jeol JSM-6490 scanning electron microscope (SEM) and a Jeol JEM-2100 transmission electron microscope (TEM). The average particle (R) and grain (d) size was measured by the chord method using GoodGrains software. The accuracy of R and d values was $\sim 10\%$ of the average value. X-ray diffraction analysis was performed using an XRD-7000 diffractometer (Shimadzu, Japan) (copper radiation, scanning step 0.02° and exposure time — 0.6 s). To identify the phases, we used data from the PDF-2 powder diffraction database and the inorganic compounds database ICSD.

2. Experimental results

2.1. Certification of powders

Fig. 1, a, b shows electron microscopic images of α-Al$_2$O$_3$ powder of series № 1. The particle size distribution of the powder is fairly homogeneous, the presence of large particles was not detected (Fig. 1, a); the average particle size is close to the manufacturer's declaration. An amorphous layer of $\sim 5-10$ nm thickness is present on the surface of submicron particles of α-Al$_2$O$_3$ (Fig. 1, b); no dislocations are detected in the crystalline lattice of particles of the № 1 series (Fig. 1, a, b).

The particle size distribution of № 2-series powders is homogeneous; the average particle size is $R \sim 0.8-1 \mu$m. The powder particles contain dislocations (Fig. 1, c).

According to the XPA results, the powders of the № 1 and № 2 series have no extrinsic phases. After mixing, the morphology of the powders does not change.

### 2.2. Electric pulse plasma sintering of powders

2.2.1. Sintering in continuous heating mode (mode A)

Figure 2 shows the dependences $\rho/\rho_{\text{th}}(T)$ for powders Al$_2$O$_3$ and Al$_2$O$_3$ + 0.5% ZrO$_2$.

The $\rho/\rho_{\text{th}}(T)$ dependencies have the usual three-stage character [15,16]. As can be seen from Fig. 2, at low heating rates ($V_h = 10$°C/min), the stage of intensive shrinkage of submicron Al$_2$O$_3$ powders lies in the temperature range 1000−1250°C and in the temperature range 1050−1450°C for the № 2 series powders. Increasing V_h for all powders leads to a shift of the $\rho/\rho_{\text{th}}(T)$ dependences to a higher
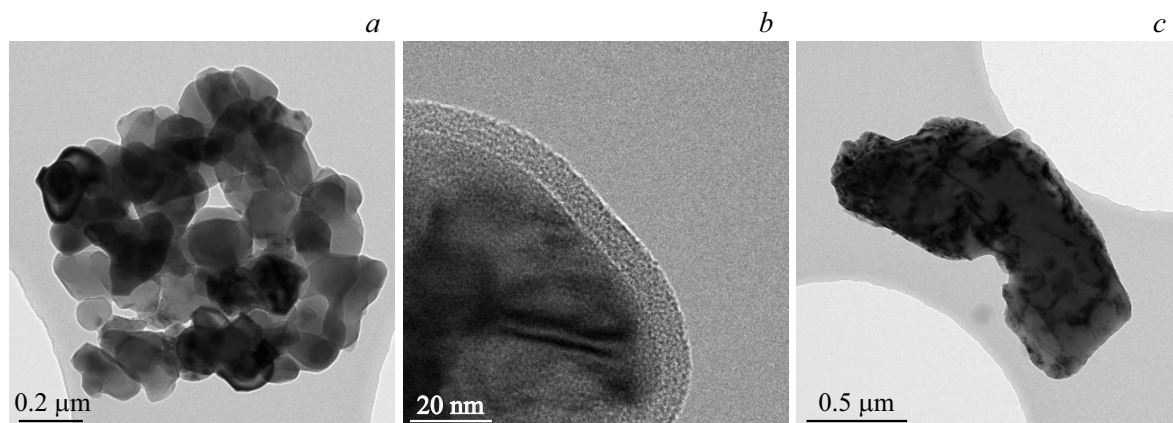
Figure 1. Electron microscopic images of powders of the № 1 (*a, b*) and № 2 (*c*) series.
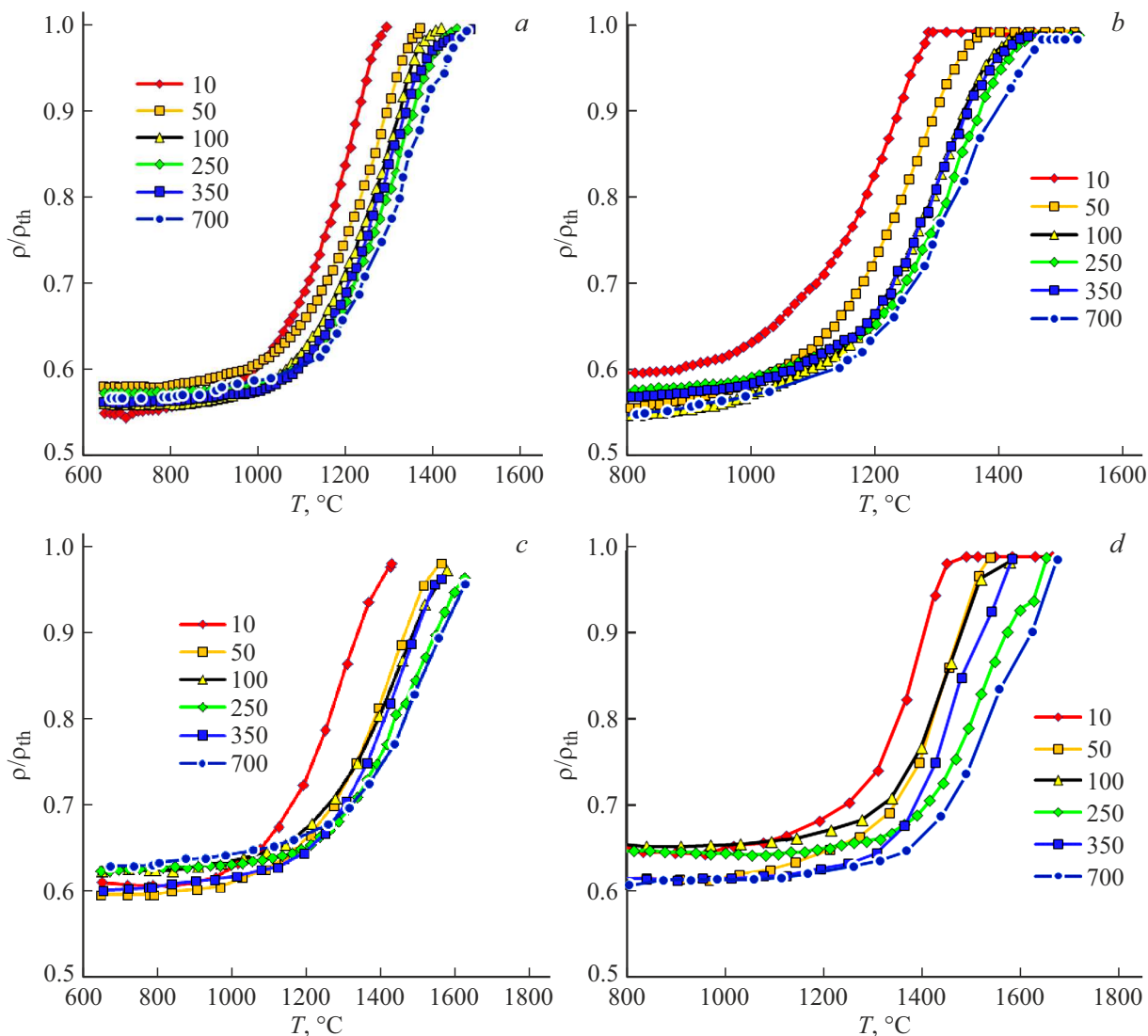
Figure 2. Dependencies of $\rho/\rho_{th}(T)$ submicron (*a, b*) and micron (*c, d*) powders Al_2O_3 (*a, c*) and $Al_2O_3 + 0.5\% ZrO_2$ (*b, d*). The heating rates (V_h) are shown in figures.

Table 1.   Properties of ceramic samples obtained by EPPS in continuous heating mode (mode A) from Al$_2$O$_3$ and Al$_2$O$_3$ powders $+ 0.5\%$ ZrO$_2$

Series	T_s, °C	V_h, °C/min	Al$_2$O$_3$				Al$_2$O$_3 + 0.5\%$ ZrO$_2$			
			d, μm	ρ/ρ_{th}, %	H_v, GPa	K_{IC}, MPa $\cdot$ m$^{1/2}$	d, μm	ρ/ρ_{th}, %	H_v, GPa	K_{IC}, MPa $\cdot$ m$^{1/2}$
1	1520	10	5.1	99.72	18.6	2.5	1.38	99.55	19.3	2.7
		50	3.0	99.67	18.2	2.3	1.18	99.49	19.6	2.8
		100	2.8	99.60	17.9	2.5	0.74	99.40	20.7	2.3
		250	2.0	99.47	17.2	2.4	0.72	99.05	20.5	2.6
		350	1.9	99.47	16.9	2.1	0.71	98.98	19.7	2.2
		700	1.8	99.28	17.8	2.4	0.72	98.48	19.1	2.6
2	1600	10	20	98.24	16.1	1.7	9.2	98.81	16.1	2.7
		50	10.6	98.14	15.9	2.1	4.7	98.72	17.2	2.9
		100	8.0	98.00	16.7	2.7	4.2	98.74	17.3	2.5
		250	6.3	97.66	17.6	2.3	3.8	98.54	17.9	3.3
		350	6.1	97.52	15.9	2.7	3.8	98.62	17.8	3.2
		700	6.1	97.20	16.7	2.5	3.8	98.53	17.6	3.1

temperature region by ~ 200°C. Fig. 2 shows that small additions of ZrO$_2$ have no effect on the nature of the dependence of $\rho/\rho_{\text{th}}(T)$. The temperature intervals of intensive shrinkage of Al$_2$O$_3$ and Al$_2$O$_3$ powders $+ 0.5\%$ ZrO$_2$ differ by no more than $20-30$°C.

Table 1 presents the results of studies of the microstructure and mechanical properties of ceramics obtained in the mode of continuous heating.

Note, the different effect of heating rate V_h and small additions of ZrO$_2$ particles on the density of ceramics of the № 1 and № 2 series. From the data presented in Table 1, it can be seen that increasing V_h leads to the expected decrease in the relative density of the ceramics. In particular, increasing V_h from 10 to 700°C/min leads to a decrease of ρ/ρ_{th} of aluminum oxide sintered from № 1 series powders from 99.72 to 99.28%, that is, the scale of density decrease is $\rho/\rho_{th} = 0.44\%$. For ceramics of No 1 series with 0.5% ZrO$_2$ addition, a similar increase V_h leads to a decrease in density by $\rho/\rho_{\text{th}} = 1.07\%$ (Table 1). Thus, increasing V_h has a stronger effect on the UMP density of Al$_2$O$_3 + 0.5\%$ ZrO$_2$ ceramic than that of pure UFG aluminum oxide. Table 1 shows that for all EPPS temperatures the density of ceramics with 0.5% ZrO$_2$ added is $\rho/\rho_{\text{th}} \sim 0.2-0.8\%$ less than the density of pure Al$_2$O$_3$ sintered in the same conditions.

In the case of EPPS powders of the № 2 series, the effect of the small addition of 0.5% ZrO$_2$ is different. First, the density of the fine-grained Al$_2$O$_3$, $+ 0.5\%$ ZrO$_2$ ceramics turns out to be $\rho/\rho_{\text{th}} \sim 0.3-1.3\%$ higher than the density of pure Al$_2$O$_3$ sintered under the same conditions. At the same time, the density of ceramics of the № 2 series is slightly lower than that of ceramics of the № 1 series.

Second, increasing the heating rate V_h from 10 to 700°C/min leads to a noticeable decrease in the density of fine-grained aluminum oxide — by more than 1% (from 98.24 to 97.20%, Table 1). At the same time, with a similar increase V_h, the density of the fine-grained Al$_2$O$_3 + 0.5\%$ ZrO$_2$ ceramic decreases by only $\rho/\rho_{\text{th}} \sim 0.3\%$. The different nature of the effect of V_h and the small addition of ZrO$_2$ on the density and grain growth in ceramics sintered from submicron and micron powders Al$_2$O$_3$ is an unexpected result.

Table 1 presents the results of microstructure studies of ceramic samples Al$_2$O$_3 + 0.5\%$ ZrO$_2$ sintered at different heating rates V_h. Note that the introduction of 0.5% ZrO$_2$ reduces the average grain size of ceramics of the № 1 and № 2 series by $2.5-3.5$ and $2.1-2.6$ times, respectively. The most significant effect on the average ceramic grain size of the addition of 0.5% ZrO$_2$ has in the case of heating with small V_h (Table 1).

During sintering of submicron powder Al$_2$O$_3 + 0.5\%$ ZrO$_2$ with small V_h anomalous grain growth — after heating to $T = 1520$°C on the background of uniform fine-grain structure with grain size $d \sim 0.7-1 \mu$m larger grains can be seen, the size of which reaches $\sim 5 \mu$m (Fig. 3, a). With increasing V_h a decrease in the size of abnormally large grains is observed, and after EPPS with $V_h = 700$°C/min the ceramics has a homogeneous UFG structure with an average grain size $d \sim 0.7 \mu$m (Fig. 3, b).

TEN results indicate that zirconium oxide particles of size $50-100$ nm are observed in the microstructure of the ceramics (Fig. 4). As can be seen from Fig. 4, the energy dispersive microanalysis of the particles indicates the
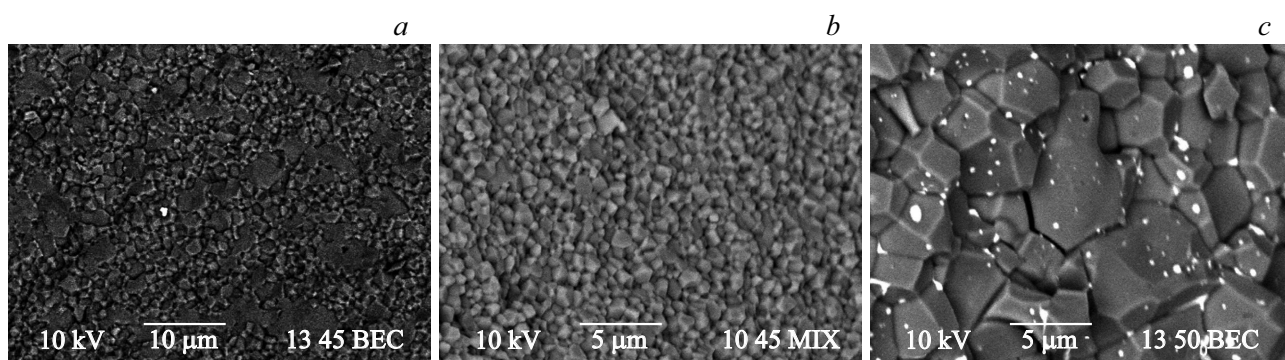
Figure 3. Fracture microstructure of ceramic samples $Al_2O_3 + 0.5\% ZrO_2$ sintered from powders series № 1 (*a, b*) and № 2 (*c*) at $V_h = 10$ (*a*) and $700°$C/min (*b, c*).
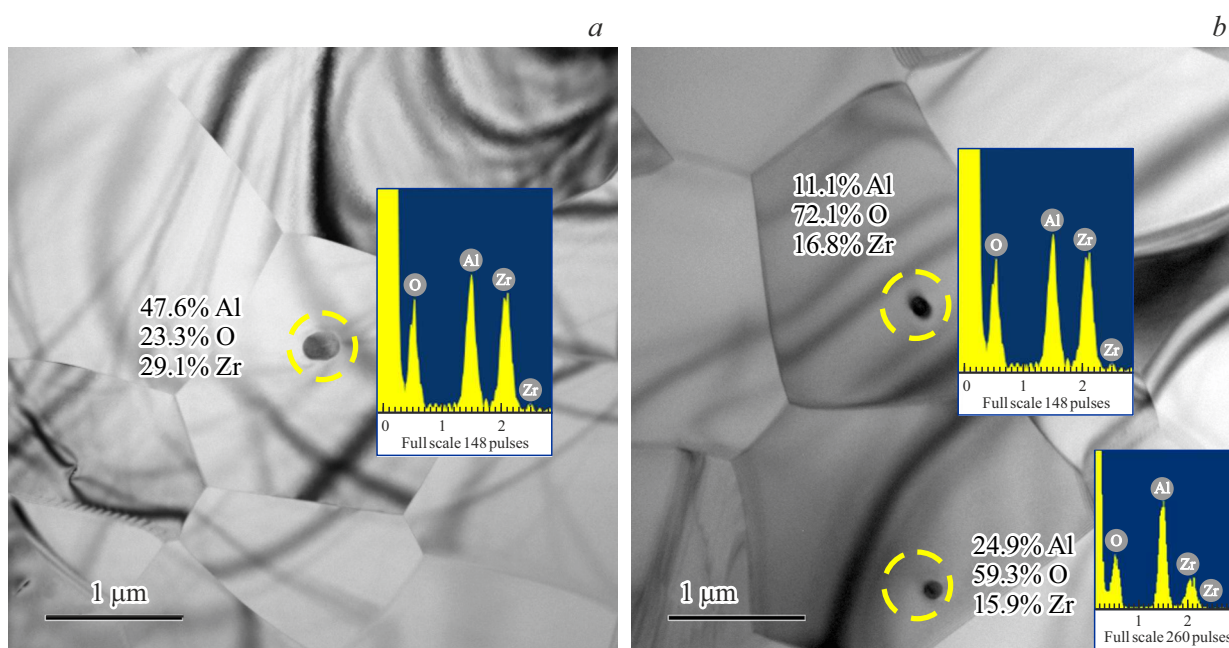
Figure 4. Microstructure of ceramics sintered from powder series № 1 at $1520°$C (different sections of the sample are represented).

presence of a clearly pronounced zirconium reflex. This indirectly indicates, that the studied particles are zirconium oxide formed as a result of grinding (abrasion) of grinding bodies (beads), which were made of stabilized zirconium oxide. The increased oxygen content, as well as the presence of an aluminum reflex, is due, in our opinion, to the wide area of excitation of the material under the electron beam, which exceeds the size of the analyzed particles. The fraction of ZrO_2 particles determined using the GoodGrains program ranges from 0.4 to 0.6−0.7%. The average fraction of ZrO_2 particles, calculated from the analysis of TEM results, is $\sim 0.5 \pm 0.1\%$.

To confirm the assumption that the observed particles are zirconium oxide, we used the XPA method.

Fig. 5 shows that the diffractogram of the ceramic has reflexes corresponding to the tetragonal phase t-ZrO_2 (PDF 00-050-1089, ICSD № 97004). The diffractogram also

shows a low-intensity reflex at $26°$, which can theoretically be attributed to the ZrAl phase (PDF 00-050-1089). At the same time, it should be noted that there are no other high-intensity reflexes of the ZrAl phase on the diffractogram (Fig. 5). Therefore, in our opinion, the reflex at $26°$ is associated with the presence of graphite (PDF 00-056-0159, ICSD № 76767) on the surface of the sample, formed by the interaction between the ceramic and the surface of the graphite mold. This assumption is indirectly supported by the fact that after additional mechanical grinding the reflex intensity at $26°$ decreased to the background level.

Quantitative phase analysis was performed by the Rietveld method in the Topas (Bruker) software package. Assuming that the impurity reflex at the diffraction angle $\sim 26°$ corresponds to graphite, the sintered ceramic was found to contain 0.6 vol.% t-ZrO_2 (0.9 mass.%) and $\sim 1\%$
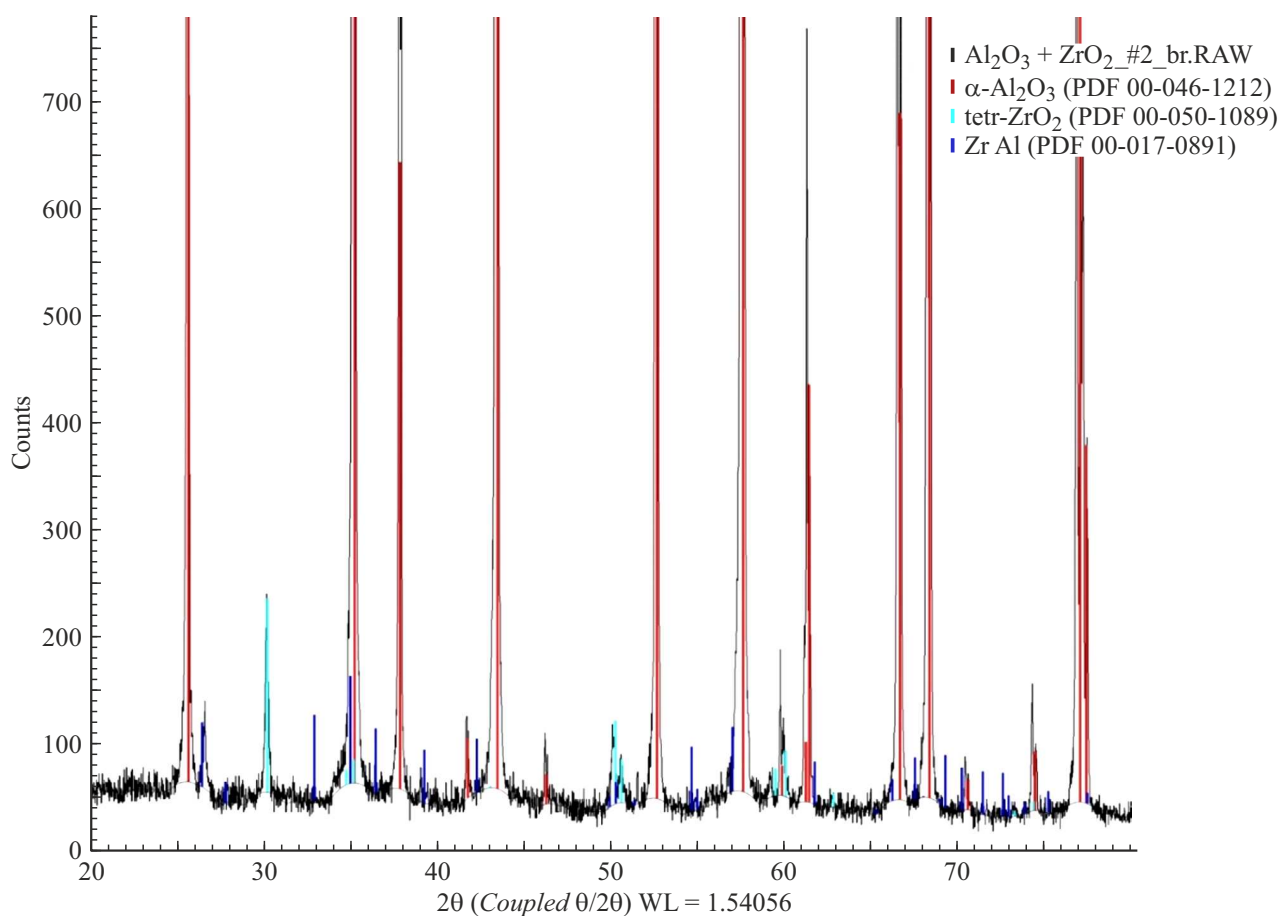
Figure 5. XPA results of Al$_2$O$_3$ + 0.5% ZrO$_2$ ceramics sintered from powder № 1 at 1520°C.

graphite. Overestimated values of the ZrO$_2$ content are due, in our opinion, to the error in determining the content of the second phase particles by XPA method.
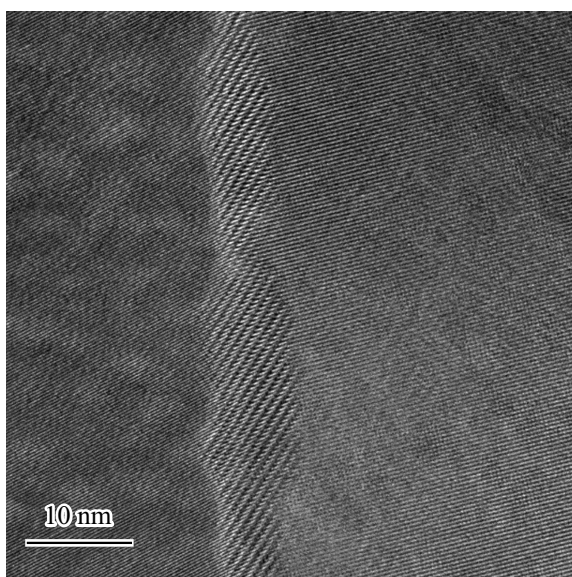
Figure 6. Structure of grain boundaries in aluminum oxide samples. Series № 1. V_h = 300°C/min.

Thus, based on the generalization of XPA and TEM results, it was found that the volume fraction of zirconium oxide particles in the ceramics under study is close to the calculated one (0.5%).

It should be noted that the sintering of powders of series № 2, which is carried out at T = 1600°C, the process of coalescence of ZrO$_2$ — fractures of samples clearly visible light submicron particles (Fig. 3, *c*). ZrO$_2$ particles are located mainly on the boundaries of aluminum oxide grains. No large ZrO2 particles are observed on the fracture surfaces of samples sintered from № 1 powder at 1520°C (Fig. 3, *a*, *b*).

It is important to emphasize that the sintering of sub-micron powders of the № 1 series results in complete crystallization of the amorphous layer located on the particle surface (Fig. 1, *b*). The results of the electron microscopic studies show that the grain boundaries of UFG ceramics have a fully crystalline structure, fragments of amorphous structure were not detected by TEM (Fig. 6).

The mechanical properties of the ceramics of the № 1 series are quite high — at V_h = 10°C/min, the hardness of Al$_2$O$_3$ + 0.5% ZrO$_2$ ceramic reaches 19.3 GPa and the crack resistance is $K_{IC} \sim 2.7$ MPa · m$^{1/2}$. Increasing V_h to 100−250°C/min increases H_v to 20.5−20.7 GPa. Heat-

Table 2. Properties of ceramic samples obtained by the EPPS method in the isothermal holding mode (mode B)

Series	T_s, °C	t_x, min	Al_2O_3				$Al_2O_3 + 0.5\% ZrO_2$			
			d, μm	ρ/ρ_{th}, %	H_v, GPa	K_{IC}, MPa·m$^{1/2}$	d, μm	ρ/ρ_{th}, %	H_v, GPa	K_{IC}, MPa·m$^{1/2}$
1	1320	0	0.2	96.26	19.5	2.3	0.2	83.24	10.7	3.6
		3	1.7	99.61	20.3	2.4	0.3	97.30	21.5	3.2
		10	2.2	99.71	19.6	2.5	0.3	99.06	22.7	3.0
		30	2.9	99.71	19.0	2.8	0.5	99.43	22.5	2.9
	1420	0	1.0	99.58	20.1	2.4	0.3	98.48	22.2	3.2
		3	4.3	99.64	18.5	2.6	0.5	99.47	21.2	3.2
		10	5.6	99.69	18.3	2.6	0.8	99.49	20.4	3.1
		30	7.6	99.72	17.3	2.9	1.4	99.52	18.9	3.2
	1520	0	2.8	99.67	18.1	2.3	0.8	99.45	20.5	3.5
		3	10.9	99.65	16.9	3.2	2.2	99.48	18.1	3.8
		10	13.4	99.66	17.5	3.0	2.8	99.51	17.6	3.4
		30	16.5	99.69	16.0	3.1	3.0	99.49	17.6	3.7
2	1470	0	1.4	96.11	17.7	2.8	–	–	–	–
		3	2.6	97.42	–	–	–	–	–	–
		10	3.9	98.02	–	–	–	–	–	–
		30	5.2	98.10	–	–	–	–	–	–
	1530	0	1.4	98.24	17.1	2.5	0.8	93.51	17.2	3.0
		3	6.1	97.93	–	–	2.1	98.24	18.5	2.8
		10	10	98.10	–	–	2.2	98.33	18.3	2.9
		30	13	98.26	–	–	2.9	98.31	17.7	3.0
	1600	0	3.8	98.14	15.9	2.1	4.2	98.72	17.3	2.5
		3	10	98.07	–	–	13	98.44	15.7	2.9
		10	15	98.15	–	–	19	98.32	16.2	2.7
		30	23	98.19	–	–	26	98.24	15.2	2.4
	1700	–	–	–	–	–	17	98.41	15.6	2.4
		–	–	–	–	–	37	98.33	15.7	3.3
		–	–	–	–	–	47	98.29	16.2	2.9
		–	–	–	–	–	52	98.14	16.1	3.2

ing with $V_h = 700$°C/min is accompanied by a decrease in the hardness of $Al_2O_3 + 0.5\% ZrO_2$ series № 1 to 19.1 GPa (Table 1). A similar effect is observed in high-speed sintering of $Al_2O_3 + 0.5\% ZrO_2$ series № 2 ceramics (Table 1). Thus, for ceramics $Al_2O_3 + 0.5\% ZrO_2$ a non-monotonic, with a maximum, character of the dependence $H_v(V_h)$ is observed.

It should be emphasized that at all V_h hardness of $Al_2O_3 + 0.5\% ZrO_2$ series № 1 is by 1−1 higher than the hardness of pure aluminum oxide, and by 1.5−2.5 GPa higher than the hardness of fine-grained ce-

ramic $Al_2O3 + 0.5\% ZrO_2$ series № 2 (Table 1). The value of K_{IC} of Al_2O_3 and $Al_2O_3 + 0.5\% ZrO_2$ ceramics is almost unchanged and is 2.2−2.8 MPa·m$^{1/2}$ (with the accuracy of determining the value K_{IC}, equal to ± 0.3 MPa·m$^{1/2}$).

2.2.2. Isothermal sintering (mode B)

Table 2 summarizes the results of studies of the density, grain size and mechanical properties of ceramics sintered in the mode B.
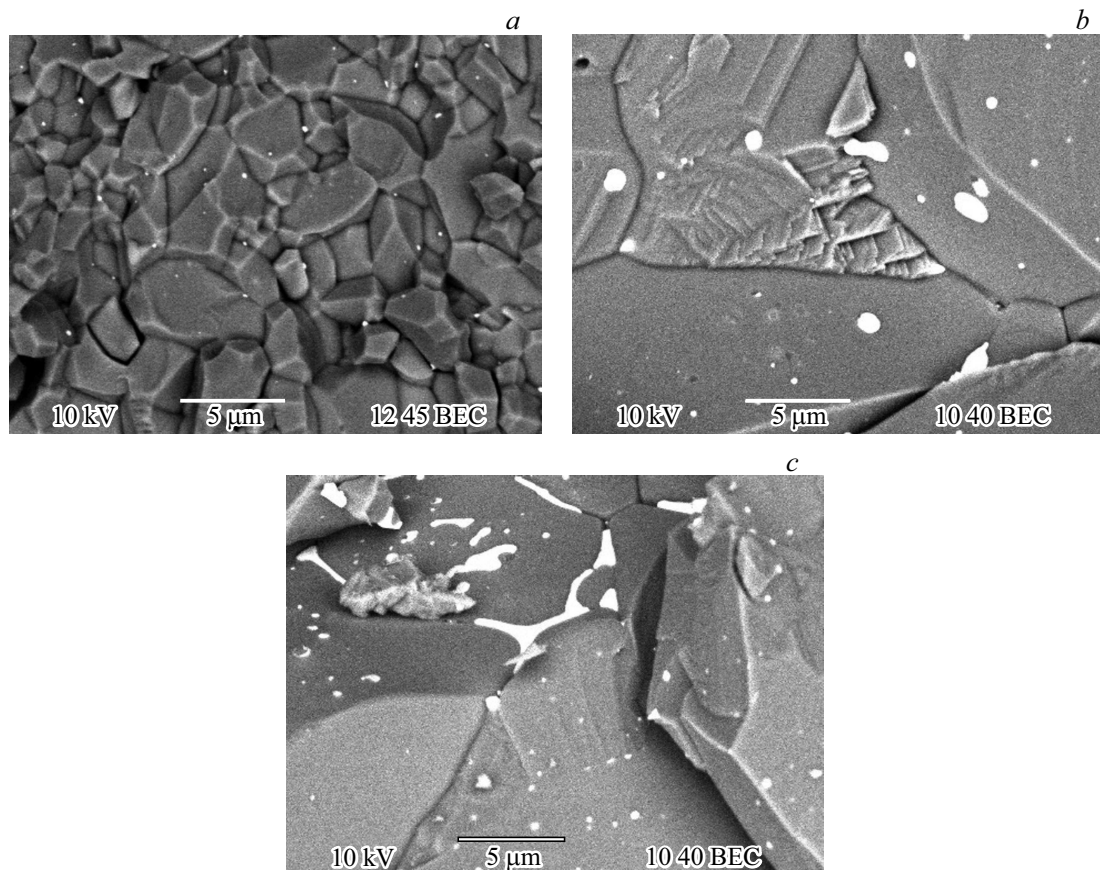
Figure 7. Fracture microstructure of ceramic samples Al$_2$O$_3$ + 0.5%, ZrO$_2$ sintered from powders of № 1 (*a*) and № 2 (*b, c*) series at $T = 1520$ (*a*) and 1600°C (*b, c*) for 30 min.

Summary of the results presented in Table 2 shows that, as in the case of sintering in the mode A, the relative density of ceramics Al$_2$O$_3$ + 0.5% ZrO$_2$ series № 1 is $\rho/\rho_{th} \sim 0.1-0.2\%$ less than the density of pure Al$_2$O$_3$. The density of Al$_2$O$_3$ + 0.5% ZrO$_2$ series № 2 is $\sim 0.2-0.3\%$ higher than that of Al$_2$O$_3$ sintered from the same powder (Table 2). Just as in the case of the A mode, the relative density of the № 1 series ceramics is higher than that of the № 2 series ceramics (Table 1, 2).

During sintering in the B mode, no abnormally large grains are observed in the structure of ceramics. Increasing the temperature and isothermal holding time leads to an increase in d (Table 2). It should be noted that the fractures of the samples show ZrO$_2$ particles whose size in the ceramics of the № 1 series does not exceed $0.1-0.2\,\mu$m (Fig. 7, *a*). Two types of particles can be observed at the grain boundaries of ceramics of the № 2 series— uniformly distributed in the volume spherical particles of size $0.5-1\mu$m (Fig. 7, it b/) and large micron particles (Fig. 7 it c), which appear only at elevated curing temperatures.

One should pay attention to the nature of grain growth in ceramics sintered in the B mode. As can be seen from Table 2, the introduction of 0.5% ZrO$_2$ additive to the submicron powder can reduce the intensity of grain growth and, as a consequence, form the UFG microstructure. A

similar effect of 0.5% ZrO$_2$ on the average grain size is observed in ceramics of № 2 series at 1530°C. In the Al$_2$O$_3$ + 0.5% ZrO$_2$ series № 2 sintered in the mode B at 1600°C, the average grain size is close to the grain size of pure Al$_2$O$_3$ considering 10% error of determination d (Table 2). We also note that when the time t_s increases from 0 to 30 min at 1600 and 1700°C, there is a slight decrease in the density by $0.27-0.48\%$ of the ceramics of the № 2 series (Table 2).

3. Summary and analysis of results

At present, a large number of physical models (see [13,15,17,18], etc.) are used to analyze the compaction kinetics of powders during EPPS.

For a preliminary description of the powder sintering kinetics at the stage of intensive compaction, the Yang−Cutler [18] model can be used. This model describes the initial stage of non-isothermal sintering of spherical particles under conditions of simultaneous processes of bulk and grain boundary diffusion, as well as plastic deformation. According to [18], the slope of the shrinkage dependence ($\varepsilon = \rho/\rho_{th}$) on temperature in coordinates $\ln(T \partial \varepsilon / \partial T) - T_m/T$ corresponds to effective activation en-

March 21, 2023 12:53 1st draft

1466　　　M.S. Boldin, A.A. Popov, A.A. Murashov, N.V. Sakharov, S.V. Shotin, A.V. Nokhrin, V.N. Chuvil'deev...

ergy of sintering mQ_s, where m — the factor depending on the dominant diffusion mechanism ($m = 1/3$ — for the case of grain boundary diffusion, $m = 1/2$ — for bulk diffusion, $m = 1$ for viscous material flow), $T_m = 2326$ K — the melting temperature of Al_2O_3. As an example, Fig. 8 shows the dependencies of $\ln(T\partial\varepsilon/\partial T) - T_m/T$ for ceramics of the № 1 and № 2 series.

Fig. 8 shows that the dependence $\ln(T\partial\varepsilon/\partial T) - T_m/T$ can be interpolated with good accuracy with a straight line at the stage of intensive compaction.

For submicron powders $Al_2O_3 + 0.5\% ZrO_2$ when increasing V_h from 10 to 700°C/min, the mQ_s value decreases from 7.1 to 6.3 kT_m. At the typical value of $m = 1/3$ [19] for fine-grained ceramic EPPS, the value Q_s lies in the range from 21.3 kT_m (411 kJ/mol) at $V_h = 10$°C/min to 18.9 kT_m (365 kJ/mol) at $V_h = 700$°C/min. The calculated values Q_s are close to the activation energy of grain boundary diffusion of oxygen in Al_2O_3 ($Q_b = 380$ kJ/mol [20]). This conclusion corresponds well with the data [13,21] that the sintering and creeping processes of aluminum oxide are controlled by the diffusion of oxygen ions along the grain boundaries Al_2O_3.

The activation energy mQ_s of micron powders $Al_2O_3 + 0.5\% ZrO_2$ is independent of V_h and is $10.8 - 13.3$ kT_m. At $m = 1/3$, the values Q_s turn out to be anomalously large and do not correspond to the known values of the activation energy of diffusion processes in Al_2O_3 [20]. At $m = 1/2$, the activation energy of EPPS is $21.6 - 29.9$ kT_m ($\sim 418 - 578$ kJ/mol). This value of Qs turns out to be intermediate between the activation energy of oxygen ion diffusion along the grain boundaries ($Q_b \sim 380$ kJ/mol [20]) and in the Al_2O_3 crystal lattice ($Q_v \sim 636$ kJ/mol [20,22]). The obtained result means that the intensity of EPPS of fine-dispersed powders $Al_2O_3 + 0.5\% ZrO_2$ is limited by simultaneous processes of bulk and grain boundary diffusion. It is likely that the increased contribution of volumetric diffusion in the EPPS of powders of the № 2 series is due to their higher sintering temperatures, as well as a larger initial particle size and, consequently, a coarser-grained structure of ceramics sintered from powders of the № 2 series.

The activation energies of EPPS of pure powders Al_2O_3 of series № 1 and № 2 are close to the activation energy of EPPS of ceramics $Al_2O_3 + 0.5\% ZrO_2$, made from these powders. In particularly, Q_s value for Al_2O_3 powders of № 1 series is $\sim 21.6 - 24.6$ kT_m (418 − 475 kJ/mol), and for powders of the № 2 series the value of $Q_s \sim 21.8 - 29$ kT_m (421 − 560 kT_m). Thus, small additions of ZrO_2 have no significant effect on the compaction mechanism of Al_2O_3 powders during EPPS. The obtained conclusion corresponds qualitatively well to the results of studies of powder shrinkage kinetics — as can be seen from Fig. 2, the addition of 0.5% ZrO_2 does not lead to a significant shift of the curves $L(T)$ in the region of low heating temperatures.

The lower values of Q_s in ceramics of the № 1 series compared to ceramics of the № 2 series are, in our opinion, due to the different state of their grain boundaries. There
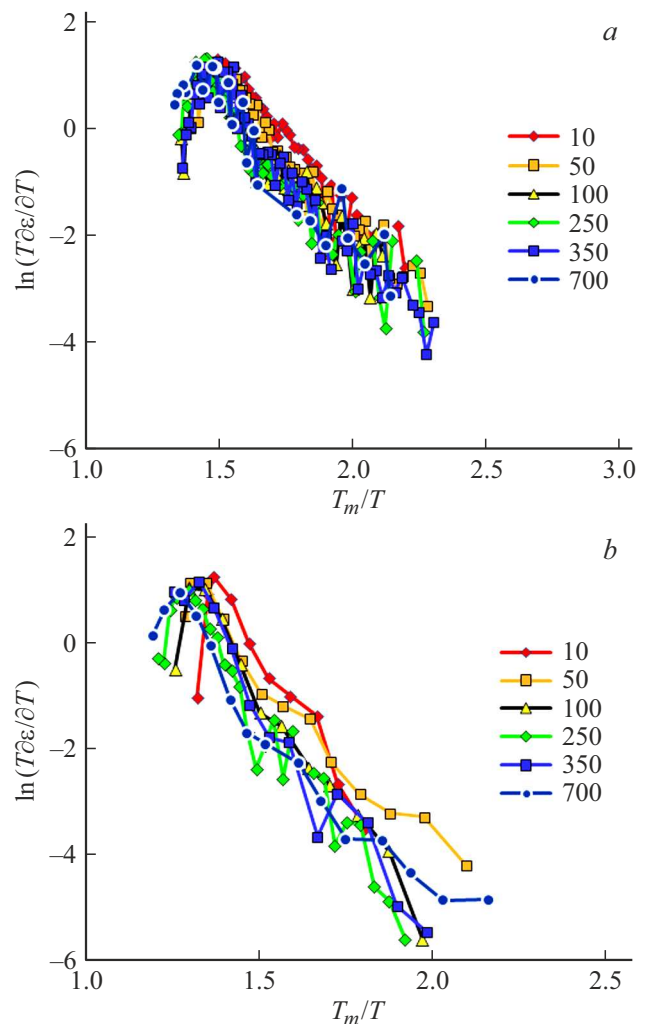
Figure 8. Dependences $\ln(T\partial\varepsilon/\partial T) - T_m/T$ for $Al_2O_3 + 0.5\% ZrO_2$ ceramic series № 1 (*a*) and № 2 (*b*).

is an amorphous layer of 10 nm thickness on the surface of powders (Fig. 1, *b*), which transforms into a crystalline grain boundary structure during sintering (Fig. 5). The structure of amorphous materials is characterized by excess free volume [23,24]. In corresponding [24], we can assume that during the transformation of the amorphous phase into the crystalline structure of the grain boundaries, defects were formed in them. These defects affect the grain boundary diffusion coefficient and the migration mobility of the grain boundaries [24]. In our opinion, the non-equilibrium state of the grain boundaries is one of the reasons for the abnormally fast grain growth during EPPS of ceramics of № 1 series, as can be seen from Table 1, the average grain size in ceramics sintered in the mode of isothermal curing at 1520°C (30 min) is $\sim 16 - 17$ μm ($\rho/\rho_{th} = 99.69\%$), and in ceramics sintered from powder series № 2 in the mode of 1530°C, 30 min, 13 μm ($\rho/\rho_{th} = 98.26\%$). The increased diffusion permeability of the grain boundaries accounts for the increased density of the № 1 series ceramics obtained in the isothermal holding

mode, as well as the observed differences in the influence of V_h on the character of the ceramic density changes. As shown above, increasing V_h from 10 to 700°C/min leads to a decrease in the density of ceramics № 1 series by $\Delta\rho/\rho_{th} = 0.44\%$ (from 99.72 to 99.28and ceramics of № 2 — by $\Delta\rho/\rho_{th} \sim 1\%$ (from 98.24 to 97.20%). It is known that the value of the diffusion coefficient along non-equilibrium grain boundaries is proportional to the density of grain boundary defects [24]. Apparently, small EPPS times allow for accelerated sintering of ceramics with nonequilibrium grain boundaries from submicron powders.

Note that the EPPS energy values are quite low compared to the activation energy of free sintering of coarse-grained $Al_2O_3-(5-95)\%$ ZrO_2 powders, which is 700 ± 100 kJ/mol, and compared to the activation energy of sintering of coarse-grained aluminum oxide $(440 \pm 45$ kJ/mol) [25]. The observed decrease in the activation energy of EPPS is, in our opinion, due to the smaller grain size in the sintered ceramics (see [26]), as well as the effect of applied pressure, whose positive effect on the acceleration of sintering is well known [1,2,17].

Let us now discuss the effect of the addition of 0.5% ZrO_2 on the growth of aluminum oxide grains.

From Tables 1 and 2 can be seen that the addition of 0.5% ZrO_2 has a significant effect on grain growth and at high heating rates can form a homogeneous UFG microstructure with grain size less than 1 μm (Table 1). The stabilizing effect of ZrO_2 particles on aluminum oxide grain growth is well known [11,12].

Note, that the smaller grain size in $Al_2O_3 + 0.5\%$ ZrO_2 ceramics compared to pure aluminum oxide should have resulted in increased density. The results of microstructure studies of samples sintered in the mode A show that the density ρ/ρ_{th} of ceramic $Al_2O_3 + 0.5\%$ ZrO_2 is less than that of pure aluminum oxide (Table 1). With increasing V_h (decreasing sintering time), there is an increase in the difference between the density ρ/ρ_{th} of aluminum oxide and ceramic $Al_2O_3 + 0.5\%$ ZrO_2 sintered in the same conditions. A similar effect is observed during sintering in the mode B — the UFG density of $Al_2O_3 + 0.5\%$ ZrO_2 ceramics is less than the density of aluminum oxide with a larger grain size (Table 2). Note also that the most significant differences in the grain microstructure of the ceramics are observed at low curing times (Table 2).

In our opinion, the ZrO_2 particles prevent compaction of ceramics at the stage of low-temperature sintering, preceding the stage of intensive compaction. This leads to a less dense press and, consequently, to a lower density of sintered ceramics. Increasing the holding time leads to more intensive sintering of UFG ceramics $Al_2O_3 + 0.5\%$ ZrO_2 and at large holding times and/or low heating rates the negative effect of ZrO_2 particles on the ceramic density is minimized due to more intense diffusion processes.

It is interesting to note that the addition of 0.5% ZrO_2 has the opposite effect on the density of aluminum oxide sintered from micron powders series № 2. As can be seen from Tables 1 and 2, the density ρ/ρ_{th} of fine-grained $Al_2O_3 + 0.5\%$ ZrO_2 ceramics appears to be greater than that of pure aluminum oxide. The reason for this is obviously the smaller grain size in $Al_2O_3 + 0.5\%$ ZrO_2 ceramics compared to pure aluminum oxide (Table 1, 2). It is important to emphasize that at elevated sintering temperatures in the mode of continuous heating or at elevated temperatures of isothermal curing in fine-grained ceramics $Al_2O_3 + 0.5\%$ ZrO_2, the processes of coalescence of ZrO_2 particles actively proceed (Fig. 3, c, 5, c). This leads to enlargement of ZrO_2 particles and reduction of the Zener inhibition force [11–14], which prevents the migration of Al_2O_3 grain boundaries. As a consequence, at elevated holding temperatures (1600°C), the average grain size of $Al_2O_3 + 0.5\%$ ZrO_2 ceramics is close to d aluminum oxide sintered from powder series № 2 (Table 2).

In our opinion, the process of coalescence of ZrO_2 particles is the reason for the decrease in the density of fine-grained $Al_2O_3 + 0.5\%$ ZrO_2 ceramics at increased high-temperature isothermal holding times. As shown in Table 2, increasing t_s from 0 to 30 min leads to a decrease in density ρ/ρ_{th} from 98.72 to 98.24% (at $T = 1600°$C) and from 98.41 to 98.14% (at $T = 1700°$C). Apparently, large ZrO_2 particles formed on the grain boundaries (Fig. 5, c) prevent sintering of ceramics.

Conclusion

The small addition (0.5 wt.%) of ZrO_2 has no noticeable effect on the kinetics of high-speed sintering of submicron and micron powders α-Al_2O_3 — values of sintering activation energy and intensive shrinkage temperature intervals for powder compositions $Al_2O_3 + 0.5\%$ ZrO_2 are close to similar parameters for pure aluminum oxide. The most significant influence on the density and average grain size of Al_2O_3 ceramics has non-equilibrium state of the grain boundaries and the process of coagulation of ZrO_2 particles. The non-equilibrium state of the grain boundaries may have a more significant effect on the intensity of boundary migration than the initial particle size Al_2O_3.

Conflict of interest

The authors declare that they have no conflict of interest.

References

[1] A.G. Evans, T.G. Langdon. *Structural Ceramics* (Pergamon Press, Oxford, 1976)

[2] V.Y. Shevchenko, S.M. Barinov. *Technical Ceramics* (Nauka, M., 1993), 192 p.

[3] A.Z.A Azhar, M.M. Ratman, Z.A. Ahmad. J. Alloys Compounds, **478** (1–2), 608 (2009). DOI: 10.1016/j.jallcom.2008.11.156

[4] J. Chai, Y. Zhu, T. Shen, Y. Liu, L. Niu, S. Li, P. Jin, M. Cui, Z. Wang. Ceramics Int., **46** (17), 27143 (2020). DOI: 10.1016/j.ceramint.2020.07.194

[5] A. Ruys. *Alumina Ceramics Biomedical and Clinical Applications* (Woodhead Publishing, Cambridge, 2019)

[6] A.P. Garshin, V.M. Gropianov, G.P. Zaitsev, S.S. Semenov. *Ceramics for Mechanical Engineering* (Nauchtehlitizdat, Moscow, 2003), 384 p.

[7] S. Meir, S. Kalabukhov, S. Hayun, Ceramics Int., **40** (8), 1287 (2014). DOI: 10.1016/j.ceramint.2014.04.059

[8] D. Jiang, D.M. Hulbert, J.D. Kuntz, U. Anselmi-Tamburini, A.K. Mukherjee. Mater. Sci. Eng. A, **463** (1–2), 89 (2007). DOI: 10.1016/j.msea.2006.07.163

[9] M. Tokita. Ceramics, **4** (2), 160 (2021). DOI: 10.3390/ceramics4020014

[10] Z.-Y. Hu, Z.-H. Zhang, X.-W. Cheng, F.-C. Wang, Y.-F. Zhang, S.-L. Li. Materials Design., **191**, 108662 (2020). DOI: 10.1016/j.matdes.2020.108662

[11] D.J. Green. J. Am. Ceramic Soc., **65** (12), 610 (1982). DOI: 10.1111/j.1151-2916.1982.tb09939.x

[12] F.F. Lange, M.M. Hirlinger. J. Am. Ceramic Soc., **67** (3), 164 (1984). DOI: 10.1111/j.1151-2916.1984.tb19734.x

[13] M.S. Boldin, A.A. Popov, E.A. Lantsev, A.V. Nokhrin, V.N. Chuvil'deev. Materials, **15** (6), 2167 (2022). DOI: 10.3390/ma15062167

[14] F.A.T. Guimarães, K.L. Silva, V. Trombini, J.J. Pierri, J.A. Rodrigues, R. Tomasi, E.M.J.A. Pallone. Ceramics Int., **35** (2), 741 (2009). DOI: 10.1016/j.ceramint.2008.02.002

[15] V.N. Chuvil'deev, M.S. Boldin, Ya.G. Dyatlova, V.I. Rumyantsev, S.S. Ordan'yan. Rus. J. Inorg. Chem., **60** (8), 987 (2015). DOI: 10.1134/S0036023615080057

[16] M.N. Rahaman. *Ceramic Processing and Sintering* (Marcel Dekker Inc., NY., 2003)

[17] E.A. Olevsky, L. Froyen. J. Am. Ceramic Soc., **92** (s1), S122 (2009). DOI: 10.1111/j.1551-2916.2008.02705.x

[18] W.S. Young, I.B. Culter. J. Am. Ceramic Soc., **53** (12), 659 (1970). DOI: 10.1111/j.1151-2916.1970.tb12036.x

[19] E.A. Lantsev, N.V. Malekhonova, Y.V. Tsvetkov, Y.V. Blagoveshchensky, V.N. Chuvil'deev, A.V. Nokhrin, M.S. Boldin, P.V. Andreev, K.E. Smetanina, N.V. Isaeva. Inorg. Mater. Appl. Res., **12** (3), 650 (2021). DOI: 10.1134/S2075113321030242

[20] H.J. Frost, M.F. Ashby. *Deformation Mechanism Maps: The Plasticity and Creep of Metals and Ceramics* (Pergamon Press, Oxford, 1982)

[21] A.E. Paladino, R.L. Coble. J. Am. Ceramic Soc., **46** (3), 133 (1963). DOI: 10.1111/j.1151-2916.1963.tb11696.x

[22] V.N. Chuvil'deev, E.S. Smirnova. Phys. Solid State, **58** (7), 1487 (2016). DOI: 10.1134/S1063783416070118

[23] V.I. Betekhtin, A.G. Kadomtsev, A.Yu. Kipyatkova, A.M. Glezer. Phys. Solid State, **40** (1), 74 (1998). DOI: 10.1134/1.1130237

[24] V.N. Chuvildeev. *Non-equilibrium grain boundaries in metals. Theory and appendices* (Fizmatlit, M., 2004), 304 c.

[25] J. Wang, R. Raj. J. Am. Ceramic Soc., **74** (8), 1959 (1991). DOI: 10.1111/j.1151-2916.1991.tb07815.x

[26] T.-S. Yeh, M.D. Sacks. J. Am. Ceramic Soc., **71** (12), C-484 (1988). DOI: 10.1111/j.1151-2916.1988.tb05812.x